Flow Measurement and Instrumentation 22 (2011) 447–455

Contents lists available at SciVerse ScienceDirect

Flow Measurement and Instrumentation

journal homepage: www.elsevier.com/locate/flowmeasinst

Bless: A fiber optic sedimeter

S. Manzoni [a], G. Crotti [b,*], F. Ballio [b], A. Cigada [a], F. Inzoli [c], E. Colombo [c]

[a] Politecnico di Milano, Department of Mechanics, Via La Masa, 1 - 20156 Milan, Italy
[b] Politecnico di Milano, Department I.I.A.R, P.za Leonardo da Vinci 32 - 20133 Milan, Italy
[c] Politecnico di Milano, Department of Energy, Via Lambruschini 4 - 20156 Milan, Italy

ARTICLE INFO

Article history:
Received 30 July 2010
Received in revised form
20 May 2011
Accepted 29 June 2011

Keywords:
Scour measurement
Bridge
Fiber optic
Bragg grating
Sedimeter
Temperature measurement

ABSTRACT

The working principle for a conceptually new sedimeter (BLESS — Bed LEvel Seeking System) is presented and experimentally tested. The proposed approach relies on the adoption of fiber Bragg grating arrays to measure temperature: the environment identification (flowing water vs. saturated soil) is achieved by means of the different temperature response to heat dissipation. The arrangement is potentially very robust with respect to the aquatic environment, as all vulnerable equipments are located above the water level, while only fiber optic and insulated electric wires with low DC voltage are immersed into water. A simple conceptual model can describe the thermodynamic response of the system. Experimental results fully confirm expectations. The technology can be considered ready for field installations.

1. Introduction

Bridge pier and abutment scour [1–5] is one of the most common causes of river bridge collapses. Scour rates and maximum depths vary with the characteristics of the system and the flow intensity; high stage conditions are typically, though not necessarily, those considered most critical for the structure stability. As the available models are unable to predict scour development with sufficient accuracy, several methods have been developed, allowing for in situ scour measurements [6–10]. Among them, echo sounders are often chosen for both transportable equipment and fixed monitoring stations: the technology is well developed both for marine and fluvial environments, they are relatively inexpensive and easy to install. However some drawbacks for use of echo sounders should be mentioned:

- when they are used in fixed installations, they must be protected against impacts of floating debris; a typical solution is to put them directly on the pier/abutment but, in such cases, special arrangements and/or high cost sensors and/or specific filtering algorithms may be required in order to prevent the sensor to be disturbed by reflections of the acoustic beam on the structure;
- accuracy of echo sounder measurements could be poor during floods due to suspended debris, bubbles and/or high turbulence within the flow [6].

The most interesting alternative to echo sounders is represented by sedimeters. These are arrays of more or less regularly spaced sensors, mounted on some supports and placed along the structure to be monitored (in some cases they are directly mounted on the structure), partially buried in the river bed and partially exposed to the flow. Many kinds of sensors can be used, sensitive to different physical variables. The only requirement is that such variable exhibits different values for the soil and for the flow, so that the interface can be identified in between two adjacent sensors showing an (abrupt) variation of the measured parameter. Literature reports present configurations adopting tell tails [11], sounding rods [6], pressure cells [12], sedimeters [6,13] and thermocouples [14]. In particular, the latter, is a sedimeter composed by thermocouples located along a low conductivity rod; the array can therefore measure the temperature profile: at the water–sediment interface an abrupt gradient is expected for situations where the two means are characterized by different temperatures.

The main advantage of sedimeters is that the sensors are not required to give accurate values of the measured quantity, as they are only asked to discriminate between the two conditions (soil, flow). Their spatial resolution is conditioned by the spacing (and, therefore, the number) of sensors along the array; however, for typical applications, high resolutions are not required. The main problem encountered so far about sedimeters is probably due to the vulnerability of the system when immersed into a dynamic aquatic environment.

In this paper the innovative sedimeter, BLESS (Bed LEvel Seeking System), based on Politecnico di Milano patent [15] is

* Corresponding author. Tel.: +39 0223996234; fax: +39 0223996298.
E-mail address: gianluca.crotti@polimi.it (G. Crotti).

0955-5986/$ – see front matter © 2011 Elsevier Ltd. All rights reserved.
doi:10.1016/j.flowmeasinst.2011.06.010

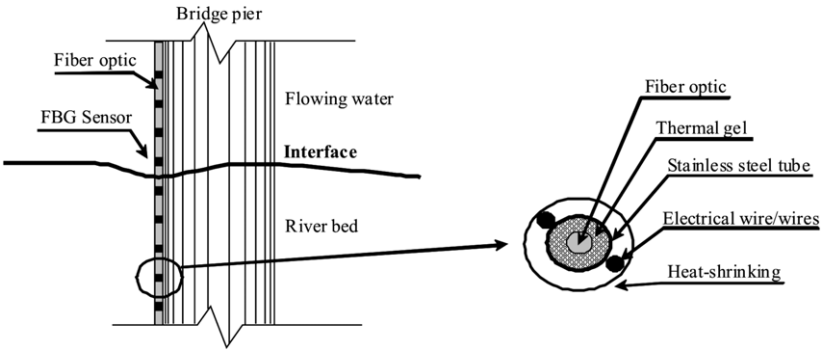

Fig. 1. Fiber optic with Bragg gratings (black squares) close to a bridge pier (left). A section of the device is shown on the right.

presented. The proposed approach relies on the adoption of fiber Bragg grating arrays to measure temperature. The arrangement is potentially very robust to survive in a harsh aquatic environment. The method is described in Section 2, focusing attention on both the working principle and its main components. Section 3 presents a simple conceptual model aimed at interpreting the dynamic behavior of the system as a function of the main control parameters. Section 4 describes the experimental set-up adopted for testing the new measurement approach in a water channel; measurement uncertainty and bias effects are analyzed in the Section 5. The last two Sections 6 and 7 are dedicated respectively to the presentation of data from the experimental campaign validating the method and a discussion of results with reference to field installations.

2. Characteristics of the monitoring system

2.1. Working principle

The basic idea is to couple an array of temperature sensors based on fiber Bragg gratings (FBG in the following) with a heat generation device: the latter is typically an electric resistor fed by an external power supply, thus producing heat by means of the Joule effect. Fig. 1 presents the system layout with reference to an installation at a bridge pier, where many different sensors are shown.

The heat produced by the Joule effect is dissipated through conduction phenomenon in the river bed and convection phenomenon in the flowing water. Due to the different efficiency of heat exchange for the two conditions, temperature sensors in flowing water should sense a lower temperature increment with respect to the surrounding temperature than those buried in the river bed as the thermal resistance is much lower for the former ones. The principle is similar to that of a hot-wire probe working with constant current [16]. It is expected that the different behavior of the two sensor families can be a reliable tool to detect the bed–flow interface. In principle, the device can be considered as an extension of sedimeters based on the measurement of natural temperature profiles across the interface [14]: such a working condition is achieved when the power dissipation unit is switched off. The possibility of heating, however, makes the system more flexible and reliable; the natural temperature difference between the flowing water and the saturated soil of the river bed varies during the day because of day/night temperature changes as well as changes in weather conditions, and seasonal variations. Therefore, a monitoring approach which only relies on natural temperature of the river system cannot guarantee reliable identification of the interface at any time. On the contrary, the addition of heat gives a further control parameter for the device, improving sensitivity, as any difference in heat exchange properties can be identified independently of the surrounding temperatures.

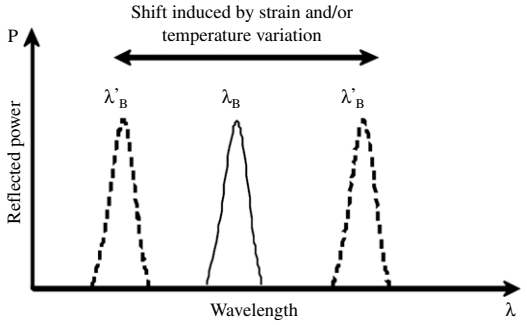

Fig. 2. Reflected light spectrum. λ_B is the Bragg wavelength and λ_B' is the generic Bragg wavelength after the shift.

2.2. Fiber Bragg grating technology

Fiber Bragg gratings can be described as wavelength-dependent filters/reflectors, when used as sensors [17]. Usually, a broad band light beam is emitted by a source into a fiber optic. When the light reaches the grating, it is partially reflected, while the remaining beam portion passes through the grating. The reflected light signal (λ_B in Fig. 2) has a very narrow spectrum. The central wavelength (Bragg wavelength) of the reflected light depends on the geometrical features of the Bragg gratings and on the refractive index [17]. A change in the grating properties involves a change of the Bragg wavelength (Fig. 2).

Bragg gratings can be adopted both for strain and temperature measurements. Temperature sensing is mostly related to the refractive index temperature dependence and, to a lesser extent, to thermal expansion. In fact, the Bragg wavelength shift $\Delta\lambda$ due to a temperature change ΔT and mechanical strain ε can be described as:

$$\frac{\Delta\lambda}{\lambda_B} = k_g(\varepsilon_m + \varepsilon_t) + \alpha_r \Delta T \tag{1}$$

where λ_B is the Bragg wavelength at the starting condition, k_g is the gage factor and α_r is the change of the refractive index per unit of temperature; the first term on the right side describes the strain impact caused by mechanical actions (ε_m) and temperature (ε_t), while the second gives the effect of a temperature change on the refractive index of glass (glass constitutes the outer part of the fiber).

As $\varepsilon_t = \beta_{\text{glass}} \Delta T$ where β_{glass} is the linear thermal expansion coefficient of the glass (glass is the main fiber component), Eq. (1) can be written as:

$$\frac{\Delta\lambda}{\lambda_B} = k_g(\varepsilon_m + \beta_{\text{glass}} \Delta T) + \alpha_r \Delta T. \tag{2}$$

Eq. (2) identifies the dependence of the central wavelength of the reflected light on temperature variation and mechanical strain;

for temperature measurements, it is essential to prevent possible strain influence on the Bragg wavelength. There are several ways to guarantee such a goal ([18] as an example). In the present case an uncoupling between thermal and strain effects has been obtained by inserting the whole fiber into a tube structure and gluing the fiber to the structure only in a single point, far away from the Bragg gratings, to grant the fiber looseness inside the sheltering envelope. This solution prevents the fiber from being affected by any strain acting on the outer structure. This solution allows mechanical resistance and protection when the tube is stressed by the river flow, without strain-related noise on the Bragg wavelength value. The very low sensitivity to any mechanical action has been verified through severe lab testing. In such a case $\varepsilon_m \cong 0$ and Eq. (2) thus becomes:

$$\frac{\Delta\lambda}{\lambda_B} = (k_g\beta_{\text{glass}} + \alpha_r)\Delta T. \tag{3}$$

Therefore, the sensor sensitivity is:

$$\frac{\Delta\lambda}{\Delta T} = (k_g\beta_{\text{glass}} + \alpha_r)\lambda_B. \tag{4}$$

Once all the parameters of Eq. (4) are known, temperature variations ΔT can be inferred from measured variation of the reflected wavelength $\Delta\lambda$. Therefore the Bragg wavelength of the reflected light is a measure of the sensor temperature. More details on fiber optic principles and temperature measurements by means of fiber optic can be found in the wide available literature ([19] as an example).

2.3. Comparison of fiber Bragg gratings with traditional temperature sensors

A great advantage of the fiber optic against other traditional temperature sensors (i.e. thermocouples and resistance temperature detectors) is that many Bragg gratings with well separated Bragg wavelengths can be inserted within a single fiber optic. This means that each Bragg grating is assigned a certain wavelength range, not superimposing the wavelength of the other sensors on the same fiber. A single optical interrogation channel can therefore be used for some tens of sensors. On the other hand, when traditional temperature sensors are adopted, each acquisition channel can be dedicated to just a single transducer.

This becomes a great advantage when the number of temperature sensors is high, in terms of system complexity and cost. This can be the case for sedimeters, as the scour level resolution depends upon the distance (and thus on the number) of temperature sensors, so that many sensors are required for an accurate measurement of the river bed level.

It is remembered that fiber optic offers the chance to have theoretically infinite resolution in temperature as well as strain detection [20], working on principles other than the FBG: however the trade-off between costs and uncertainty required by the particular application is to the advantage of FBG sensors.

FBGs have many further advantages against traditional temperature sensors. First of all, light flows in the fibers instead of electrical power, thus having electromagnetic interference immunity, no possibility of short circuits, etc. The fibers are then a very thin dielectric, which can be hidden to preserve their mechanical integrity. A further fundamental advantage of FBGs is that only fiber optics are immersed in water, while all the vulnerable electric and electronic components can be safely hosted over the river surface. Fiber optic performances are only weakly affected by the presence of water, giving a stable output provided the strain effects are avoided. Therefore, the proposed measurement system offers a much higher reliability and robustness, if compared to more traditional ones.

3. Conceptual model

For a typical device configuration, the energy transfer capabilities are different from location to location; sensors perceive different local temperatures as a consequence of the thermal properties of the surrounding environment: the portion of the device immersed in the flowing water is interested by convective heat transfer phenomena while the portion immersed in the river bed is primarily interested by conduction heat transfer to the saturated soil. Physical processes will be modeled in the 2D transversal plane only, since the measurement device has a large extension in the vertical direction compared with the two dimensions in its cross section.

Let us idealize the system as a cylinder of finite radius containing both the fiber and the heat generation wire. Assuming constant heat dissipation per unit length of fiber $\dot{Q}$ on the device, the energy conservation law for the part immersed in the fluid can be written as:

$$\begin{cases} M_d c_d \dfrac{\mathrm{d}T_w}{\mathrm{d}t} = \dot{Q} - hS_d(T_w - T_{ow}) \\ t = 0 \quad T_w = T_{ow} \end{cases} \tag{5}$$

where M_d, c_d and S_d are mass per unit length, specific heat and convective surface per unit length of the cylindrical stainless steel tube respectively, h is the heat transfer coefficient, T_w is the sensor temperature in flowing water, T_{ow} is the far field fluid temperature and t is time. The Equation set (5) implicitly assumes that the initial temperature of the fiber is equal to that of the fluid: the assumption will simplify the resulting relations and is adequate for the following discussion. Introducing a reduced temperature $\Delta T_w = T_w - T_{ow}$, Eq. (5) reduces to a linear, first-order, non-homogeneous, differential equation whose general integral is:

$$\begin{aligned} &\Delta T_w = \Delta_Q\left(1 - \mathrm{e}^{-t/\tau}\right) \\ &\text{with: } \tau = \frac{M_d c_d}{hS_d}; \qquad \Delta_Q = \frac{\dot{Q}}{hS_d}. \end{aligned} \tag{6}$$

Eq. (6) gives the transient temperature of a sensor immersed in flowing water expressed as a function of the convective heat transfer coefficient and power supply: for $t \to \infty$ the difference ΔT_w between the sensor and fluid temperature tends to the values Δ_Q imposed by the heat dissipation; the transient is exponential with time constant τ which is a function of probe characteristics (material and geometry) and convective heat transfer coefficient.

For the array portion buried in the saturated soil it is convenient to approximate the system as a cylinder of vanishing radius; in such case the temperature distribution around the measurement device is obtained integrating the partial differential equation describing a conductive heat transfer process from a concentrated linear source:

$$\begin{cases} \dfrac{1}{a_s}\dfrac{\partial T_s}{\partial t} = \dfrac{1}{r}\dfrac{\partial}{\partial r}\left(r\dfrac{\partial T_s}{\partial r}\right) \\ t = 0\ r > 0 \quad T_s = T_{os} \\ t > 0\ r = 0 \quad -k_s S_d \dfrac{\partial T_s}{\partial r} = \dot{Q} \end{cases} \tag{7}$$

where r is the radial distance from the heat source; a_s and k_s are the thermal diffusivity and thermal conductivity of the soil, respectively; T_s is the temperature of the fiber in the soil, T_{os} is the undisturbed soil temperature. The initial temperature for the fiber equals that of the surrounding soil. After introducing the reduced temperature $\Delta T_s = T_s - T_{os}$, the solution of the differential problem (7) is:

$$\Delta T_s = \frac{\dot{Q}}{4\pi k_s}\int_{r^2/4a_s t}^{\infty} \frac{\mathrm{e}^{-u}}{u}\mathrm{d}u. \tag{8}$$

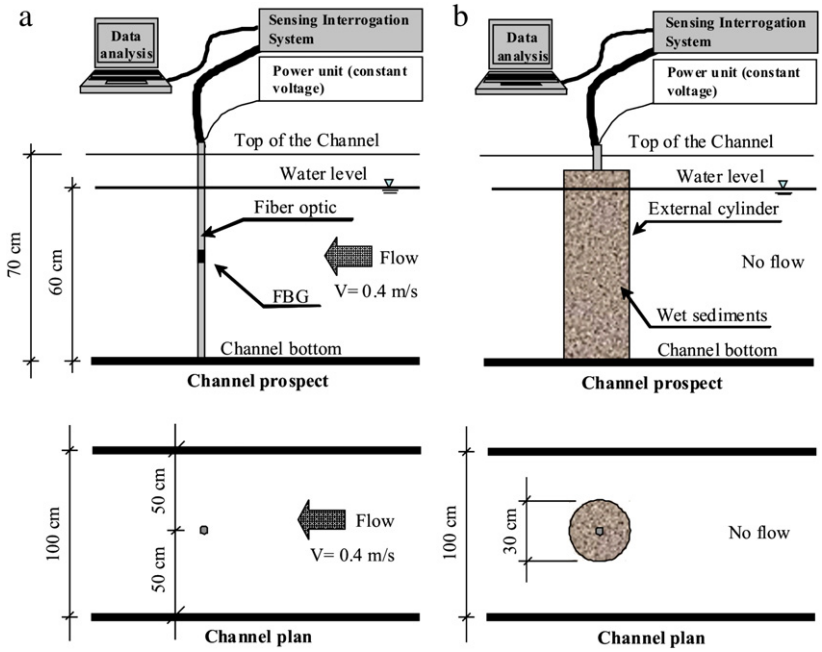

Fig. 3. Layout of laboratory tests. Sensors in flowing water (a) and buried in wet sediments (b). Figures not to scale.

The integral on the right side of Eq. (8) is the exponential integral function. In accordance with [21], for $u < 0.01$ ($t > 10$ s for the tests discussed in the next sections), Eq. (8) can be approximated as:

$$\Delta T_s \cong \frac{\dot{Q}}{4\pi k_s}\left[\ln\left(\frac{4a_s t}{r^2}\right) - \gamma\right] = \alpha_Q\left[\ln\left(\frac{t}{\vartheta}\right) - \gamma\right] \quad \text{with: } \vartheta = \frac{r^2}{4a_s}; \qquad \alpha_Q = \frac{\dot{Q}}{4\pi k_s} \tag{9}$$

where γ is the Euler–Mascheroni constant ($\gamma = 0.5772$). Differently from the convection governed solution (6), temperature indefinitely grows with a logarithmic trend starting from its initial value T_{os}; the (logarithmic) growth rate being proportional to the heat dissipation rate.

Eqs. (6) and (8)–(9) directly express the characteristics of the measuring system, and its capability of detecting whether the probes are facing the flowing fluid or the saturated soil. By subtracting Eqs. (9) and (6) one obtains the (approximate) relation:

$$\Delta\Delta T_{sw} = \Delta T_s - \Delta T_w \cong \dot{Q}\left[\frac{\ln\frac{t}{\vartheta} - \gamma}{4\pi k_s} - \frac{1 - e^{\frac{-t}{\tau}}}{hS_d}\right] \tag{10}$$

where $\Delta T_s - \Delta T_w$ is the difference of temperature gap for the portions of fiber facing the soil and the fluid with respect to the far field temperatures for the two conditions. Such quantity can be used to detect the river bed–fluid interface. It is important to notice that, given the intrinsic and geometric characteristics of the environment and of the device, $\Delta\Delta T_{sw}$ is an increasing function of time and, for any given instant, it can be varied by varying the heat flux. Therefore, it is always possible to overcome the unavoidable disturbances and system heterogeneities by choosing proper time and heat flux values which make $\Delta\Delta T_{sw}$ large enough, so that the interface can be robustly identified. When the heat flux per unit length $\dot{Q}$ is set to zero we have $\Delta\Delta T_{sw} = 0$ and, therefore, $T_s - T_w = T_{os} - T_{ow}$; that is, the array is able to identify the interface as far as the difference of the undisturbed temperatures of the soil and the water is large enough to be detected by the sensors (same working principle as in [14]).

As a conclusion of the section, it is important to underline that the equations presented here are essentially intended as interpretative more than predictive models for the measuring system: it is clear that the quantitative behavior of the system is conditioned by the parameters contained in Eqs. (5) and (7), whose values can be only approximately estimated *a priori*. This is especially true for the heat transfer coefficient h, which depends on the flow characteristics and the local geometry of the system, and for thermal diffusivity and conductivity of the soil.

The mentioned equations provide a tool for sensitivity analysis, defining the strength effect of each parameter on the final measurement. Moreover, explicit solutions like those in Eqs. (6) and (9) are valid only within the relatively simplified hypotheses which have been applied here, while deviations from the behaviors expressed by such solutions can be expected due to a variety of reasons (first of all the three dimensions of the real system). In spite of all these limitations, the obtained solutions, condensed in Eq. (10), explicitly indicate an expected linear dependence of $\Delta\Delta T_{sw} = \Delta T_s - \Delta T_w$ on the heat flux and a relatively complex dependence on time, which are sufficient to ensure that the system can work under varying (and uncertain) external conditions; such results should be considered as the essential contribution of the conceptual model to the monitoring system. The analyses presented in Sections 5 and 6 will clarify the discussion.

4. Experimental tests

The tests have been performed in the Hydraulics laboratory at Politecnico di Milano. There are two experimental set-up facilities (Fig. 3):

- *sensor immersed in flowing water*, Fig. 3(a). A water channel with width and height equal to 100 and 70 cm respectively has been used. The water level was 60 cm and the average velocity of the flow was 0.4 m/s. The fiber was immersed in flowing water;
- *buried sensor*, Fig. 3(b). An external cylinder was added and filled with sediments saturated with water, as the geometry of a sensor attached to the buried portion of a pier foundation was simulated.

At the preliminary stage a fiber optic (single mode SMF-28) equipped with just a single FBG was used (Fig. 4). As mentioned, the fiber was embedded in a stainless steel tube (with a diameter of

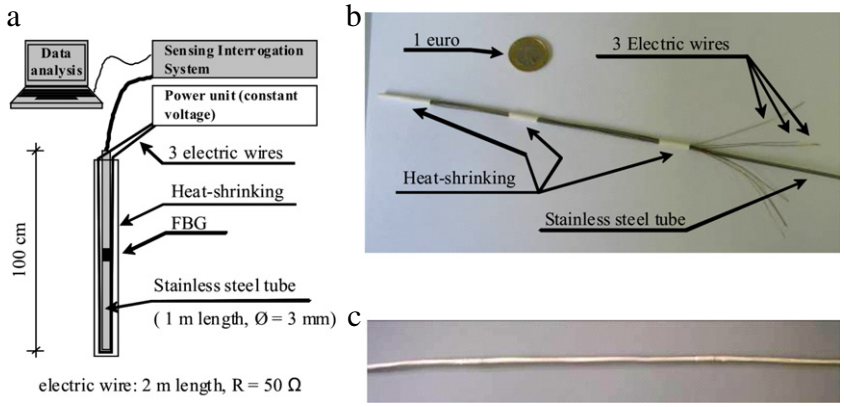

Fig. 4. Tested device. Main device components (a), configuration of the tested device (b) and final layout of the tested device (c).

Table 1
Test nomenclatures.

Dissipated power $\dot{Q}$ (W/m)	Test code, flowing water	Test code, wet sediments
0	1w	1s
0.5	2w	2s
1.0	3w	3s
1.5	4w	4s
2.0	5w	5s
4.0	6w	6s
4.5	7w	7s
6.0	8w	8s
8.0	9w	9s
9.0	10w	10s
12.5	11w	11s
13.5	12w	12s
16.0	13w	13s
16.8	14w	14s
24.0	15w	15s
25.0	16w	16s
33.6	17w	17s
37.5	18w	18s
50.5	19w	19s

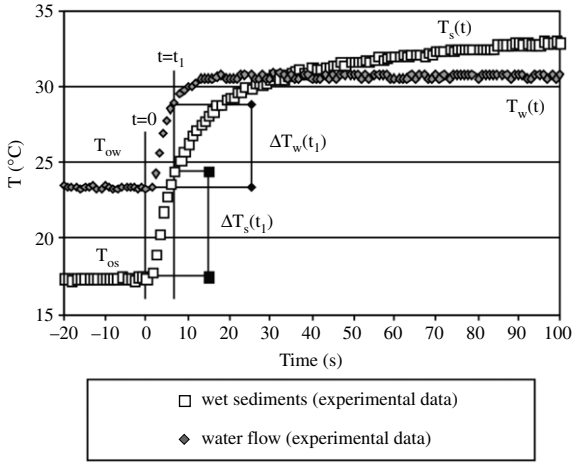

Fig. 5. Sensor response in different environments. Test 19 of Table 1. $t < 0$ — sensor measures the temperature of the environments (T_{ow} in flowing water and T_{os} in wet sediments); $t > 0$ — power unit is turned on.

3 mm). The interrogation system worked in the wavelength range between 1510 and 1590 nm. Three electrical wires were placed along the steel tube, connected to a power unit supplying a constant voltage within the range (0–29 V). Each wire covered the tube length twice (from the top to the bottom and backwards) with a total length of 2 m and a total resistance of 50 Ω. The use of multiple electric wires allowed for an easier modulation of the dissipated heat flux. The contact between the tube and the electric circuit was guaranteed by heat-shrinking; in the final configuration the heat-shrinking covered the whole fiber.

Experiments were carried out for constant values of all parameters with the exception of the dissipated power which was varied in the range 0 → 50.5 W/m (Table 1). All tests were started from equilibrium condition, where no power was dissipated, then followed by a stepwise increase of the power up to the nominal value for the specific test, with a typical duration of 100 s. Fig. 5 shows typical time histories for temperatures in water and saturated soil (test 19, refer to Table 1); time $t = 0$ corresponds to the heating onset; further comments will be given in Section 5.

5. Metrological qualification

A crucial issue to be discussed for the present application is related to measurement uncertainty and accuracy. As previously discussed, the main variables used for the interface identification are the temperature differences ΔT_s and ΔT_w, which are affected by uncertainty and eventual bias effects. These two factors are discussed separately in Sections 5.1 (uncertainty) and 5.2 (bias effects). A further important aspect is the uncertainty linked to the identification of the interface. This is faced in Section 5.3.

5.1. Temperature measurement uncertainty

The first issue to be discussed is that of measurement uncertainty due to random effects. Two different uncertainty sources have to be accounted for: FBG sensor and sensing interrogation system intrinsic uncertainty. FBG sensor uncertainty u_{fbg} (with a confidence level of 66% [22]) is declared as 0.6 °C by the manufacturer. The sensing system manufacturer declares an uncertainty u_s (with a confidence level of 66%) of 1 pm (the physical variable sensed by the interrogation system is wavelength). Considering that the used FBG sensors have a sensitivity Ri of about 10 pm/°C, 1 pm corresponds to 0.1 °C. Relying on the uncertainty propagation law [22], the total uncertainty u to be associated to temperature measurements is:

$$u = \sqrt{u_{\text{fbg}}^2 + \left(\frac{u_s}{Ri}\right)^2} = 0.61\ ^\circ\text{C}. \tag{11}$$

This uncertainty u has again a confidence level of 66%. Therefore, when T is the measured temperature, the corresponding range of possible temperature values with a confidence level of 66% is $T \pm u$. Corresponding uncertainties for temperature differences $\Delta T = T_1 - T_2$ can therefore be evaluated as:

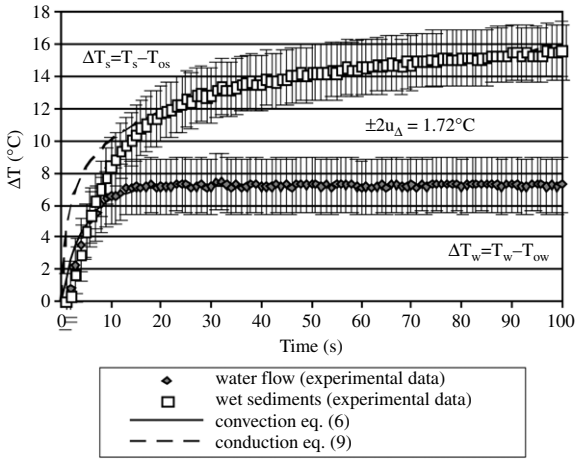

Fig. 6. Temperature differences derived from time series of Fig. 5 with the theoretical equation of convection (6) and conduction (9) heat transfer. Uncertainty intervals $\pm 2u_\Delta$ are ± 1.72 °C.

$$u_\Delta = \sqrt{\left(\frac{\partial \Delta T}{\partial T_1} u\right)^2 + \left(\frac{\partial \Delta T}{\partial T_2} u\right)^2} = \sqrt{(u)^2 + (-u)^2} = 0.86\ ^\circ\text{C}. \tag{12}$$

Actually, experimental tests carried out by the authors have shown that this value is overestimated. The adopted FBGs (coupled to the used sensing interrogation system) show a lower uncertainty value. Nevertheless, the computed value will be used in the following as a conservative hypothesis.

Fig. 6 shows temperature differences derived from time series of Fig. 5 and the related uncertainty intervals $\pm 2u_\Delta = \pm 1.72$ °C, corresponding to a confidence level of 95% [22]. Although the intervals appear to be exaggeratedly wide with respect to the actual scatter of the measured values, after a relatively short time it is still possible to unambiguously detect which sensor is in water and which in the soil.

5.2. Bias effects for temperature measurement

A bias effect results in a systematic error in temperature measurement. This means that the measured temperature is different from the real one and that this difference responds to a fixed law.

If temperature differences ΔT are considered, the bias effect typically tends to become lower or even to disappear, thanks to the subtraction. This has been experimentally checked by the authors on tens of FBGs. In most cases the bias effect on temperature difference is small and negligible with respect to the uncertainty associated to temperature differences (i.e. ± 1.72 °C). When this is not verified it is possible to recalibrate the sensor to eliminate the bias effect. Therefore, bias effects are assumed to be a minor issue in this application, being negligible in terms of method reliability.

5.3. Scour depth estimation uncertainty

Temperature measurement uncertainty has been accounted for so far. Once it is assured to recognize sensors in water and soil, the uncertainty linked to the position of the interface has to be discussed. The optical fiber manufacturer declares that FBG position can be located within a symmetric interval as large as 10 mm (called *range* in Eq. (13)); on the basis of direct controls over fibers with lengths up to 30 m, we were able to check that an interval of ± 5 mm around the nominal position for the sensor location is a conservative assumption. Thus, the uncertainty u_p on sensor position can be estimated as (type B uncertainty [22]):

$$u_P = \frac{\text{range}}{2\sqrt{3}} = \frac{10}{2\sqrt{3}} = 2.9\ \text{mm}. \tag{13}$$

Supposing that the required resolution *res* (i.e. sensor spacing) is 1 m, u_p can be neglected and it is straightforward to conclude that the water/soil interface is located between two consecutive sensors, thus with a maximum approximation of half of the resolution *res*. Nevertheless, a further specific case deserves attention. This is when a sensor is just in correspondence of the interface. In such a case its data can become difficult to be comprehended so that the two close FBGs have to be used to discover the scour level. This means that approximation grows up in this case. A similar issue takes place when a single FBG grating fails its measurements (or gives wrong data) because it is damaged. The basic idea is to have an array of sensors and it is thus easy to recognize sensors giving unreliable data. In such a case it is enough to avoid considering data from such a sensor, although this causes a spatial resolution worsening. The past history of a single grating and of the close sensors can help in solving ambiguous situations.

6. Results

Figs. 5 and 6 respectively show the time histories of temperatures $T(t)$ and temperature variations $\Delta T(t) = T(t) - T_o$, for sensors in the two different environments, as a response to a positive step of heat flux at time $t = 0$ ($\dot{Q} = 0 \rightarrow 50.5$ W/m, tests 19w and 19s of Table 1). Notice that, in this test, the base temperatures for the two phases (negative times: $T = T_{os}, T_{ow}$) differ enough from each other to clearly distinguish the phases also in the absence of heating; however, such a condition is not guaranteed in field measurements, where temperature differences between the flow and the river may be too small and typically change sign between night and day conditions. When the system is heated the sensor rapidly reaches a constant temperature value when immersed in flowing water, while temperature continuously rises, although at decreasing rates, when immersed in the saturated soil. The behavior is qualitatively and quantitatively coherent with Eqs. (6) and (9), which are also plotted in Fig. 6 for proper values of the corresponding parameters (Δ_Q, τ) and (α_Q, ϑ) (values are discussed below). Notice that Eq. (9) is expected to hold only for "long" times; this motivates the evident data deviation at the beginning of the investigated phenomenon. Moreover, the mathematical model of heat transfer in soil is simplified by the assumption of linear heat source. The experimental device has a proper thermal inertia that justified the different behavior during the initial time. Regardless of the better or worse adaptation of experimental results to the expected trends, after a short initial transient of about $5 \div 10$ s the two signals become clearly distinguishable: as expected, values for the sensor immersed in the soil are steadily larger than those for the sensor immersed in flowing water.

Table 2 reports the quantitative values for all parameters in Eqs. (6) and (9) for the case of Fig. 6. The geometrical dimension of the probe and its thermophysical quantities have been defined according to the probe manufacturer. The convective heat transfer coefficient h and the thermo-physical properties of the ground are evaluated according to literature [23]. While evaluating the adaptation of the analytical models to experimental results, it should be considered that the calibration exercise for the scales (Δ_Q, τ) and (α_Q, ϑ) highly benefits from the relatively wide range of acceptable values for some of parameters which are combined into such scales. Individual calibration of the thermodynamic parameters is out of the scope of this work. In fact, the only important property to be proven is that such parameters are not dependent on temperature levels and heat fluxes for given physical conditions. From the analysis of all time series, it has been verified that (6) and (9) fit the experimental data for all tests of Table 1

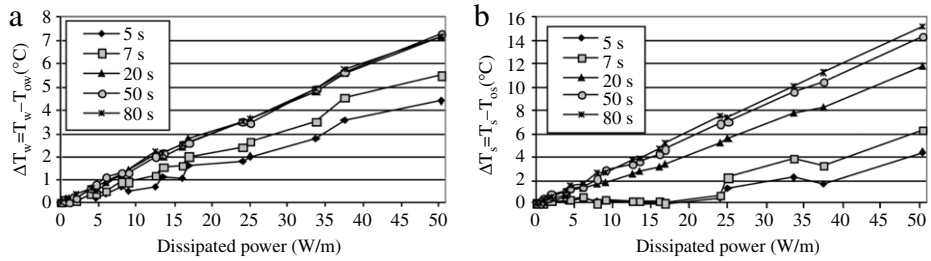

Fig. 7. Temperature variation against the dissipation power per unit length for 5 time series. In flowing water (a), in saturated soil (b).

Table 2
Quantitative values for parameters in Eqs. (6) and (9).

Convection (Eq. (6))			
Physical parameters	M_d	0.0132	kg/m
	c_d	2200	J/(kg K)
	S_d	0.0125	m^2/m
	h	530	$W/(m^2 K)$
	$\dot{Q}$	50.5	W/m
Scales of equation	Δ_Q	7.2	°C
	τ	4.5	s
Conduction (Eq. (9))			
Physical parameters	r_d	0.002	m
	γ	0.5772	–
	a_s	0.00001	m^2/s
	k_s	1.61	W/(m K)
	$\dot{Q}$	50.5	W/m
Scales of equation	α_Q	2.5	°C
	ϑ	0.1	s

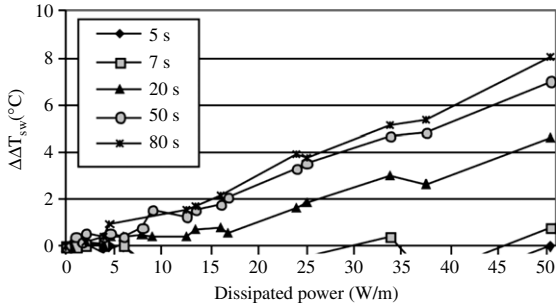

Fig. 8. $\Delta\Delta T_{sw}$ difference between curves of Fig. 7(b) and (a).

for the same set of values for all physical parameters, as given in Table 2. A (partial) proof of such a result is demonstrated in Figs. 7 and 8 which show the dependence of the temperature variation ΔT as a function of the dissipated power per unit length $\dot{Q}$ for different instants along the time series. Fig. 7(a) (sensor in flowing water) clearly shows that the relation $\Delta T = \Delta T(\dot{Q})$ is linear for all values of the time, as expected from Eq. (6). Fig. 7(b) (sensor in saturated soil) shows a similar trend for the higher time values, while some anomalies are evident for the shortest times; this is, again, coherent with the conceptual model previously described.

Finally, Fig. 8 plots the difference between the two temperature variation, $\Delta\Delta T_{sw} = \Delta T_s - \Delta T_w$, which is also a (linearly) increasing function of the dissipated power, at least for the larger time values (Eq. (10)). The interface can be unambiguously located between two subsequent sensors (along a sedimeter) given that $\Delta\Delta T_{sw}$ exceeds a proper threshold, defined on the basis of the measurement uncertainty and of the intrinsic physical non-homogeneity of the system to be measured; in other words, the principal variables ΔT_s and ΔT_w must be different enough to recognize differences due to two phases (fluid, soil) with respect to the scatter of the data along a line of sensors forming the sedimeter. Fig. 8 indicates that for the tested configuration such conditions can be achieved only for values of the dissipated power larger then 20 W/m; the minimum duration for the heating which guarantees that $\Delta\Delta T_{sw}$ exceeds the threshold is inversely correlated with the dissipated power.

Results are synthesized in Fig. 9 where contour lines for $\Delta\Delta T_{sw}$ are plotted in a time–dissipated power (per unit length) plane (log–log axes). Experimental points are not shown for the sake of clarity of the picture. Experimental contour lines are superimposed with theoretical lines of Eq. (10) for time values larger than 15 s, while for smaller times Eq. (10) departs from measured values. The chart in Fig. 9 can be used for the design of the measuring system: $\Delta\Delta T_{sw}$ must exceed the minimum value for identification of the different behavior of the two environments; values for $\Delta\Delta T_{sw}$ larger than the threshold allow for robust localization of the interface. Once the requested level for $\Delta\Delta T_{sw}$ is fixed, possible couples $(t, \dot{Q})$ are identified. As is obvious, one can choose a lower level of power so far the duration of the dissipation is long enough. If shorter times are wished (for example, because higher time resolution is requested), $\dot{Q}$ must be increased. The

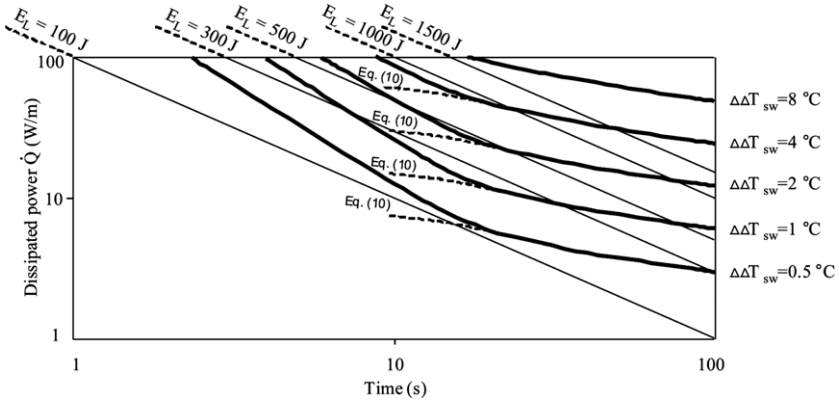

Fig. 9. Contour lines for $\Delta\Delta T_{sw}$ on a time–dissipated power domain. Isoenergetic lines are also plotted.

levels of constant dissipated energy per unit length $E_L = \dot{Q} \cdot t$ are also plotted in the chart. Fig. 9 indicates that, typically, minimum energy configurations are reached for short pulses of intense dissipation. This information can be particularly useful for systems powered by solar panels, where energy consumption may be critical.

7. Discussion

Expectations on the behavior of the system are confirmed by experimental results. In particular:

- the response to heat scattering is clearly different for sensors in flowing water and sensors in saturated soil; this allows to identify transitions between the two environments;
- the difference of temperature increases as a response to heat scattering grows with time and with the dissipated power.

The conceptual model presented in Section 3 is able to predict such trends with a good degree of approximation. Non-uniform environmental conditions (especially within the soil) and/or measurement uncertainties can be overcome by setting the system parameters $(t, \dot{Q})$ so that the difference $\Delta\Delta T_{sw}$ is large enough to emerge over the irregularities of the measured temperatures along the sedimeter.

It should be also noticed that, so far, we have analyzed the instantaneous temperature increase difference $\Delta\Delta T_{sw}$ to detect the sediment–water interface. However, this is not the only possible working principle for the proposed sedimeter; alternatives are shortly discussed below:

- the system can be used as in [14], i.e. by not dissipating any power along the sedimeter, and using the natural temperature gradient at the interface (where/when present) to identify it;
- heat dissipation forces different behaviors in the two environments, whose differences are not limited to the level of temperature increase; their temporal gradients are also different so that the rate of temperature increase could be a useful indicator too;
- various strategies of dissipating heat along time could also be considered as alternatives to simple positive or negative steps;
- more in general, the joint use of more indicators and/or modalities of use of the system could make the identification more robust.

An important point of this system (as well of any sedimeter as scour measuring device) is that the working principle is not based on the measurement of a single sensor but on the comparison of the responses of an array of sensors in space (i.e. comparison among the sensors at a given time) and time (i.e. comparison of the behavior of a single sensor at different times), which makes the identification very robust also in the absence of specific calibration and validation. Fiber optic sensors make such a property even more powerful: a single sensor is relatively inexpensive and inherently robust to the water environment, while all the expensive and vulnerable components are safely positioned over the water level and one single interrogation channel is needed for tens of sensors.

Herein, only the general system characteristics have been discussed and analyzed. Several further parameters require specification with respect to field applications. Examples are:

- geometry of the pier/abutment and position of the sedimeter with respect to it;
- applications different from bridge structures: for example, the system could be used to monitor bed aggradation/degradation along river reaches in towns, as flood risk is connected to such phenomena; another application is monitoring check dams during high stage events;
- geometry of a support for the sedimeter, in order to fix it to the bridge structure and protect it from dynamic loads;
- alternative configurations for temperature sensors (the stainless steel tube is only one of the possibilities offered on the market);
- electric wires with variable resistance, in order to concentrate the heat flux in front of the sensor and therefore reduce the total dissipated power.

Although not reported here, we have tested the system under some of the listed alternatives: quantitative values are always affected by the specific conditions but the overall performance of the system, that is its capability of detecting differences between flowing water and saturated sediments, is basically unaffected by them. A first prototype field installation has been already built on a road bridge over the River Po, Italy; only preliminary results are available, but they fully confirm that the sedimeter can properly identify the bed level around the piers.

Conclusions

The working principle for a conceptually new sedimeter, based on fiber optic technology has been tested. The system is based on the identification of the environment (flowing water vs. saturated soil) by means of the difference in temperature response to heat dissipation. Experimental results fully confirm expectations. A very simplified conceptual model is able to explain the main features of the system, especially with respect to its response to the intensity and duration of the heat scatter, which is one of the main control parameter of the technology, as it permits to amplify the differences of the thermodynamic response across the interface between the two environments.

We consider the technology to be ready for field applications; prototype installations are in progress.

References

[1] Melville BW. Local scour at bridge abutments. Journal of Hydraulic Engineering 1992;118(4):615–31.
[2] Melville BW. Pier and abutment scour: integrated approach. Journal of Hydraulic Engineering 1997;123(2):125–36.
[3] Cardoso AH. Effect of time and channel geometry on scour at bridge abutments. Journal of Hydraulic Engineering 1999;125(4):388–99.
[4] Johnson PA. Comparison of pier-scour equations using field data. Journal of Hydraulic Engineering 1995;121(8):626–9.
[5] Melville BW, Coleman SE. Bridge scour. Water Resources Publications; 2000.
[6] National Cooperative Highway Research Program. NCHRP. Report 396—instrumentation for measuring scour at bridge piers and abutments. Transportation Board and National Research Council. 1997.
[7] De Falco F, Mele R. The monitoring of bridges for scour by sonar and sedimetry. Independent Nondestructive Testing and Evaluation International 2002;35(2):117–23.
[8] Radice A, Ballio F. A non-touch sensor for local scour measurements. Journal of Hydraulic Engineering 2003;41(1):105–8.
[9] Lin Y-B, Chen J-C, Chang K-C, Chern J-C, Lai J-S. Real-time monitoring of local scour by using fiber Bragg grating sensors. Smart Materials and Structures 2005;14:664–70.
[10] Lo K-F, Ni S-H, Huang Y-H, Zhou X-M. Measurement of unknown bridge foundation depth by parallel seismic method. Experimental Techniques 2009;33(1):23–7.
[11] The HR Wallingford scour monitoring system. Wallingford (Oxon, UK): Bridge Assessment Management and Design, HR Wallingford Ltd.; 1994.
[12] Rickly hydrological company. http://www.rickly.com/ss/scoursensor.htm.
[13] Yung BL, Jihn SL, Kuo CC, Lu SL. Flood scour monitoring system using fiber Bragg grating sensors. Smart Materials and Structures 2006;15(6):1950. doi:10.1088/0964-1726/15/6/051.
[14] Camp CV, Pezeshk S, Leatherwood TD. Detecting bridge scour by thermal variation across the stream bed. In: Proceedings of the international water resources engineering conference. 1998. p. 246–51.
[15] Cigada A, Ballio F, Inzoli F. Hydraulic Monitoring Unit. Application for international patent no. PCT/EP2008/059075. 2008.

[16] Doebelin EO. Measurement systems: application and design. 5th ed. The McGraw-Hill Companies; 2004.
[17] Hill KO, Meltz G. Fiber Bragg grating technology fundamentals and overview. Journal of Lightwave Technology 1997;15(8):1263–76.
[18] James SW, Dockney ML, Tatam RP. Simultaneous independent temperature and strain measurement using in-fibre Bragg grating sensors. Electronics Letters 1996;32(2):1133–4.
[19] Measures RM. Structural monitoring with fiber optic technology. Academic Press; 2001.
[20] Sayde C, Gregory C, Gil-Rodriguez M, Tufillaro N, Tyler S, van de Giesen N, et al. Feasibility of soil moisture monitoring with heated fiber optics. Water Resources Research 2010;46:W06201. doi:10.1029/2009WR007846.
[21] Tseng P-H, Lee T-C. Numerical evaluation of exponential integral: Theis well function approximation. Journal of Hydrology 1998;205:38–51.
[22] Uncertainty of measurement—part 3 guide to the expression of uncertainty in measurement. ISO/IEC Guide 98-3:2008. GUM:1995.
[23] Warren M, Rohsenow WM, Hartnett P, Cho YI. Handbook of heat transfer. 3rd ed. New York: McGraw-Hill; 1998.